Acoustic Emission Spectroscopy

Acoustic emission (AE) spectroscopy has become the method of choice in many fieldsbecause it is highly sensitive. For example, the AE system constructed by the Vallen company, Germany, has a sampling rate that can reach up to 10 MHz, an arrival time resolution of 100 ns, and an energy resolution of $1.8 \times 10^{-18} V2s$ (i.e., in the attojoule regime, aJ) referred to sensor signal at 34 dB preamplifier gain.

1. Introduction

Geotectonic processes are often perceived as slow, encapsulated in the colloquial expression of 'long geological time scales'. With improved experimental facilities to identify the details of geological time dependences, we now understand that they occur on many different time scales. Even those which evolve over thousands of years, such as some metamorphic processes, proceed by short-time atomistic changes which simply add up to the observed long-term evolution. Long-term time evolution is often constituted by a long sequence of short singular events and research has partly shifted from the continuous description of geological processes to the analysis of these singular events from spontaneous changes in chemical composition, atomic ordering, phase transitions, and crack propagation to earthquakes, the collapse of structures in the mining industry and so forth. The investigation of singular 'rare events' has entered geological and mineralogical research after it already became a key research field in metallurgy [1][2], material sciences [3][4][5] and solid-state physics [6][7][8]. In addition, many short events are commonly observed in biogenic materials and in food processing. The observation of the collapse of these materials under stress leads to novel analytical tools to register the collapse mechanisms via the formation of avalanches and allow an assessment of their mechanical stability.

2. Avalanches and Acoustic Emission Spectroscopy

When physical systems produce discontinuous burst responses under external fields, the bursts often follow the predictions of avalanche physics and 'crackling noise' emitters [6][9][10]. Typical examples include natural avalanche disasters, such as earthquakes [11][12]. The avalanche behavior does not depend on the size of the earthquake with pico-scale earthquakes and global earthquakes following very similar patterns. Avalanche dynamics also describe the fluctuations of stock markets, which have small fluctuations and stock disasters caused by financial crisis [6], the temporary evolution of neuron connectors during 'thinking' processes [13][14][15], and the medical deterioration of brain structures [16][17]. Other examples are the Barkhausen 'noise' of pinned domain walls during magnetization processes [18][19][20][21], martensitic transformations [22][23], plastic deformation in solids [24], materials failure [25], ferroelectric and ferroelastic domain movements [3][26][27][28][29] etc. Avalanche events are monitored by different monitoring methods, such as force drop measurement [30], optical observation [28], thermal radiation observation [23], etc.

Acoustic emission (AE) spectroscopy has become the method of choice in many fields [5][31][32][33] because it is highly sensitive. For example, the AE system constructed by the Vallen company, Germany, has a sampling rate that can reach up to 10 MHz, an arrival time resolution of 100 ns, and an energy resolution of $1.8 \times 10^{-18} V2s$ (i.e., in the attojoule regime, aJ) referred to sensor signal at 34 dB preamplifier gain. A previous study showed simultaneous measurements of the avalanche of stress and AE during mechanically induced twin boundary motion in a shape memory alloy. It showed that the probability of finding an AE event during a stress drop is ~100 times higher than between stress drops. Additionally, the relations between mechanical energy drops and the lower bound of the acoustic emitted energy is approximately proportional [34]. The common drawback of AE is that the local signal is first locally transferred into an acoustic signal inside the sample which then propagates as an acoustic wavelet to the noise detector. The wave profile of AE is hence determined only indirectly by the initial signal and great care has to be taken not to confuse the measured signal with that of the initial atomic event. This problem has been analyzed in great detail [35], the analytical techniques highlight the strong similarity with the deconvolution procedure to analyze propagating waves in the context of geophysical

seismology. The current statistical analysis of AE signals, especially its energy probability distribution function (PDF) and the interevent times, are not much affected by wave profiles and there is a large amount of literature which elucidates some of the intricacies of AE spectroscopy [35][36][37][38]. The AE signal is in the form of a wave in **Figure 1** , and the important parameters of AE waves are their amplitude, duration, rise time, absolute energy, and waiting time.
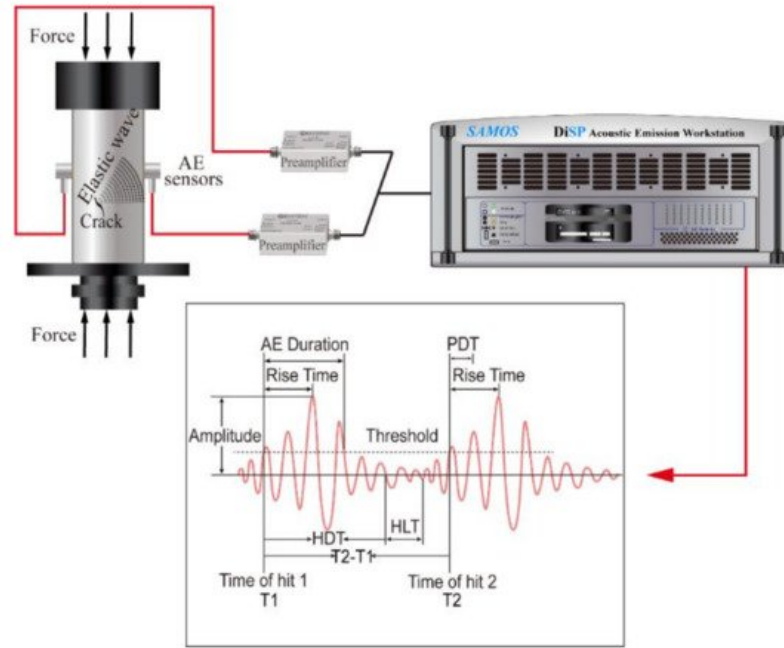

Figure 1. Schematic typical AE experiment and AE signals. The setting of the Peak Definition Time (PDT) ensures correct identification of the signal peak for rise time and peak amplitude measurements. If the PDT is smaller than the rise time, the amplitude captured by AE system would be smaller than the truth value. Proper setting of the Hit Definition Time (HDT) ensures that each AE signal from the structure is reported as one and only one hit. If the HDT is larger than (T2-T1), hit 1 and hit 2 will be detected by AE system as just one hit. AE system needs HLT to get ready for the next signal detection, with proper setting of the Hit Lockout Time (HLT), spurious measurements during the signal decay are avoided and data acquisition speed can be increased.

The amplitude A(t) is a function of time t and captures the evolution of the conjugate parameter to the external force. The time evolution of the amplitude is typically initiated by an incubation period where A(t) increases exponentially leading to the maximum amplitude, called A max . The duration is the time period over which an avalanche survives. Experimental time scales typically extend from a few microseconds to many milliseconds. Absolute energies are obtained by numerical integration of the square voltage of signals $E = 1/R \int_{t_i}^{t_j} U^2 t \, dt$, where t_i and t_j are starting and ending times of the signal and R = 10 kΩ is a reference resistance. The rise time is the time difference between starting time of a wavelet and time of the wave peak. The waiting times are the times between consecutive events, also called 'interevent times'.

3. Avalanche Mixing

A crucial outcome of previous research is that failure does generally not follow a single mechanism. This surprising result can be exemplified by the observation of a collapse processes in metals [2] where local porous collapse and the movement of dislocations combine to achieve the final, global collapse. In other cases, the porous collapse entails the avalanche movements of twin boundaries [39], or a phase transition triggers catastrophic changes of microstructures related to structural transformations [40]. During avalanche evolution we find that often one instability triggers another instability. This means that several avalanche mechanisms interact and mix dynamically [41]. In this situation, probability densities are no longer simple power laws but show the typical up-wards curvature of mixed power laws [42]. Salje et al. [42] extended the analysis of mixing to the use of the 'maximum likelihood estimation method', ML [43][44][45]. They derived the characteristic ML profiles for single, underdamped avalanches (a plateau), a damped avalanche (a monotonically increasing profile), and mixed avalanches (a peak before a plateau). The upwards bent probability density distribution translates into a steep increase in the ML estimates for small avalanche energies which peaks at a maximum value, which is bounded by the energy exponent of the avalanche with the higher exponent. It then decays towards the exponent of the second avalanche. This rather complex ML profile was identified in several experimental investigations, which shows that avalanche mixing is indeed a much more common phenomenon than previously assumed [6].

In order to confirm the mixing mechanism for different avalanches during a collapse process, Salje and his coauthors designed a simple and instructive experimental arrangement. They used two materials with different strengths and superimposed them in the same stress device (**Figure 2**) [46]. The stress was identical for both materials, but the avalanche dynamics were different. This experiment combined one porous material at the early stage of uncorrelated, random damage mode while the second material was more highly damaged within the correlated failure state. The common stress created two avalanche processes simultaneously and ensured mixing between them. In the compression experiment, they used coal and sandstone as test materials. As predicted by theory, the probability distribution of the AE energy of the composite rock was a nonpower law with an upwards bent of the probability distribution function (PDF) in double logarithmic display. The maximum likelihood estimation curve showed the predicted increase, peak and decrease towards the lower exponent (**Figure 3**). Several other compression experiments show that the mixing effect of different avalanche mechanisms is a common phenomenon. For example, compression experiments on granite show that the crumbling and fracture mechanism of granite mineral particles can form a state of avalanche mixing [47]. High temperature annealing (near the α-β phase transition temperature of quartz) reduces the internal constraints of granite and weakens the effect of fracture, so that the mixing between crumbles and fracture is observed (**Figure 4**). The AE crack analysis helps to evaluate whether there is prior damage in granite, which plays an important role in the safety assessment of granite caves for nuclear waste deposition.
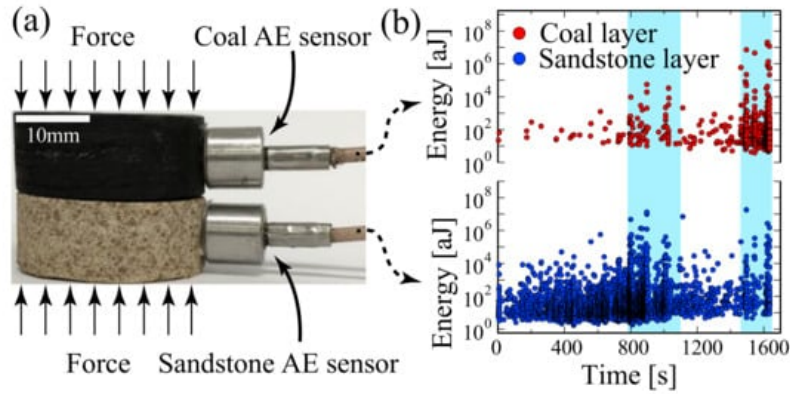

Figure 2. (**a**) Experimental arrangement for high stress measurements. (**b**) Energies of AE hits, detected by the transducers attached to coal and sandstone as indicated by their color as function of time. This experiment contains 1001 events in coal, and 4875 events in sandstone. The shadowed areas indicate time intervals from 790 s to 1100 s and from 1460 s to 1635 s. Reproduced with permission from [46]. American Physical Society, 2019.
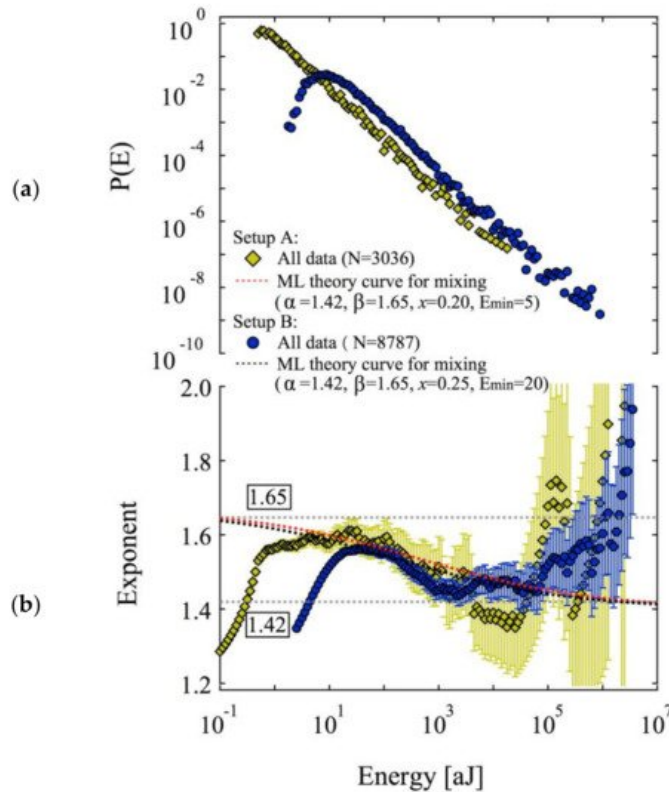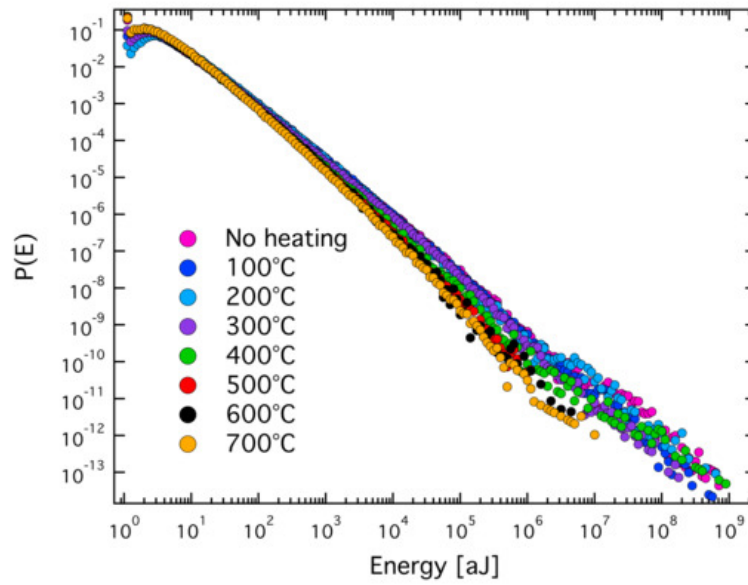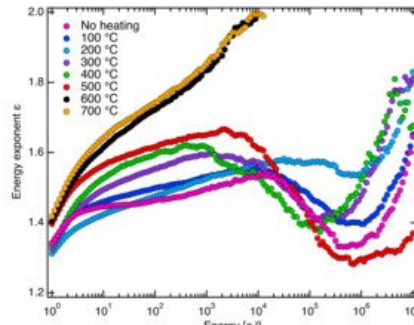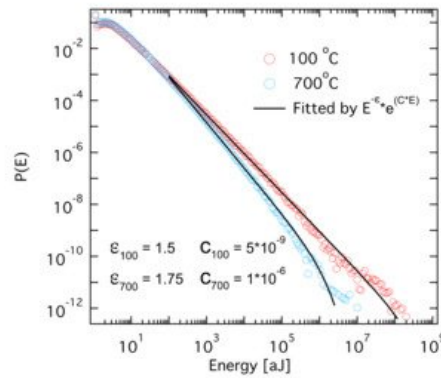
Figure 3. Log–log histogram of energy distributions (**a**), and ML analysis of the power law exponent as a function of a moving threshold (**b**) for sandwiches of sandstone and coal. 'Setup A' indicates low stress measurements, 'Setup B' high stress measurements. Reproduced with permission from [46]. American Physical Society, 2019.

(a)

(b)

(c)

Figure 4. (**a**) Distribution of avalanche absolute energies for different temperatures. (**b**) The ML-fitting exponent ε as a function of a lower threshold E_{min}. (**c**) Damping and pure power fitting for the distribution of avalanche absolute energies of 100 °C and 700 °C. Reproduced with permission from [47]. De Gruyter, 2019.

For uniaxial compression under stress control, the sample compression stops after the first cracks occur. If the stress is further increased, it constitutes a confining effect and additional friction occurs. This effect was exemplified for sandstone where confined compression tests always show avalanche mixing, in contrast with the uniaxial compression test without confinement [48].

In addition to geological materials, the mixing of different avalanche mechanisms has also been studied in several materials. For example, in a porous Mg-Ho alloy, the interaction between dislocation and fracture leads to the mixing of avalanche mechanism during compression and tension [2]. The critical exponents of the two mechanisms are consistent with the mean field theory and the force integrated mean field theory, respectively. Furthermore, the two avalanche

mechanisms can be separated by synchronous waveform analysis. Chen and her collaborators have demonstrated how to separate dislocation moves and entanglements in 316 L stainless steel. They showed that the main difference between the two mechanisms is the average duration for each type of avalanche [49].

4. Applications

The energy consumption to produce cement for building work is particularly high. The cement industry creates significant environmental pollution, so that the development of new environmentally friendly cementitious materials has become a research hotspot in many countries. Some micro-organisms produce calcium carbonate in the process of metabolism, which induce calcium carbonate deposition during cementation [50][51]. One of the important applications is in the construction of calcareous sand islands and reefs. Calcareous sand exists widely throughout the Earth's tropical zones. The main construction requirement is that calcareous sand needs to be reinforced for foundation construction. Wang et.al. carried out compression failure experiments on single calcareous sand grain, unconsolidated sands and biocemented sand block [52] (see **Figure 5**). All three materials show avalanches under compression. Through the analysis of the avalanche characteristics of the three samples, it was found that the destruction mechanism of the biocemented calcareous sand is the failure of the bonding between sand particles via the biogenic calcium carbonate. Under stress the biocemented calcareous sand blocks degenerate rapidly back into sands without cementation and some carbonate clusters. In this case, the observation of crackling noise provides an excellent indicator for the stability of biocemented structures.
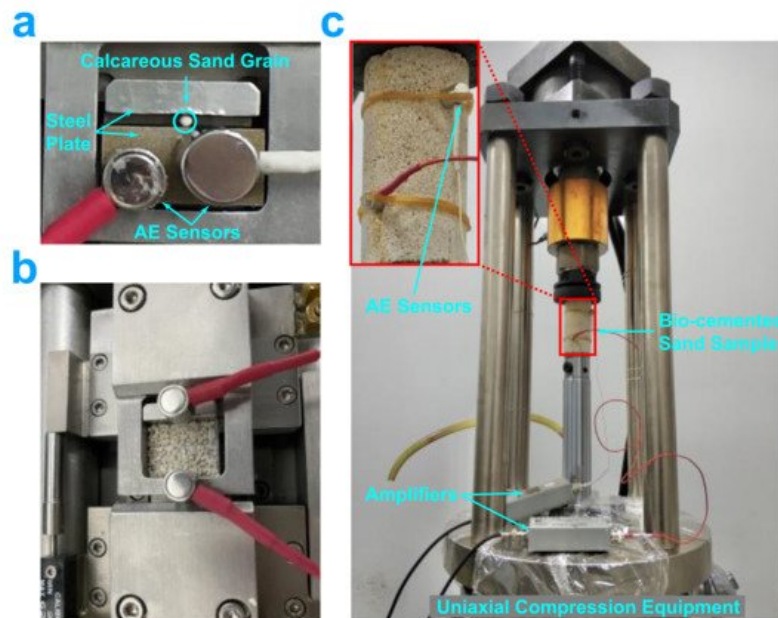

Figure 5. Compression arrangement for (**a**) grain, (**b**) sands without cementation, and (**c**) biocemented sand sample crushing. Reproduced with permission from [52]. Elsevier, 2021.

Teeth are the strongest part of the human body. They not only have the function of chewing, but also play an important role in pronunciation and facial appearances. They also contain microcracks which are not routinely found by optical and CT examination in dental clinics. This leads to wrong diagnosis of crack formation before the cracks become large enough to be observed optically. Moreover, tooth cracks do not self-repair, they can induce periodontitis and, ultimately, the loss of the tooth. The cracks do not induce pain at the initial stage, making it difficult for patients to detect tooth damage. When pain occurs, the best opportunity for treatment has already been missed. Wang et al. used healthy human molars to carry out damage examinations and found that the process of tooth cracking displays obvious avalanche characteristics [53]. Human teeth are composed of hydroxyapatite from a nanometer to a micrometer scale and are typically brittle. Cracks progresses through the tooth dentin pores, and exhibit abundant microstructures such as crack bridging, crack deflection and crack bifurcation. This complex crack evolution leads to avalanche dynamics. The stress–strain curve is a typically serrated with clustering of the acoustic emission signal. The absolute energy of AE meets the power-law distribution over nearly seven energy decades with a power-law exponent $\varepsilon = 1.4$, **Figure 5** . The statistical distributions of signal amplitudes, durations, correlations between energies and amplitudes, and the relationship between amplitude and duration all meet the prediction of mean field theory very well. These avalanche signals do not appear when the tooth is undamaged so that the acoustic emission method is a warning of developing microcracks in teeth.

When a constant force is applied to a material it still transforms via creep. Even if the applied force is lower than the ultimate strength of the material, the material will still fail after long-term damage accumulation. Creep is predominant in geotechnical and geological engineering, so it is necessary to monitor creep and predict disaster accumulation over time. According to the creep failure experiment of sandstone [54], it is found that the acoustic emission signal is weaker in the stable creep stage than under constant strain rates. When the failure is approaching collapse, the AE signal of creep shows a series of activity periods (**Figure 6**), which is different from the AE signal of increasing uniaxial compression. The probability density distribution of AE in the first few cycles has a high critical exponent value of $\varepsilon = 1.6$–1.7, while the final failure shows a fracture exponent of $\varepsilon = 1.4$. This creep results are consistent with fiber bundle simulations [55][56].
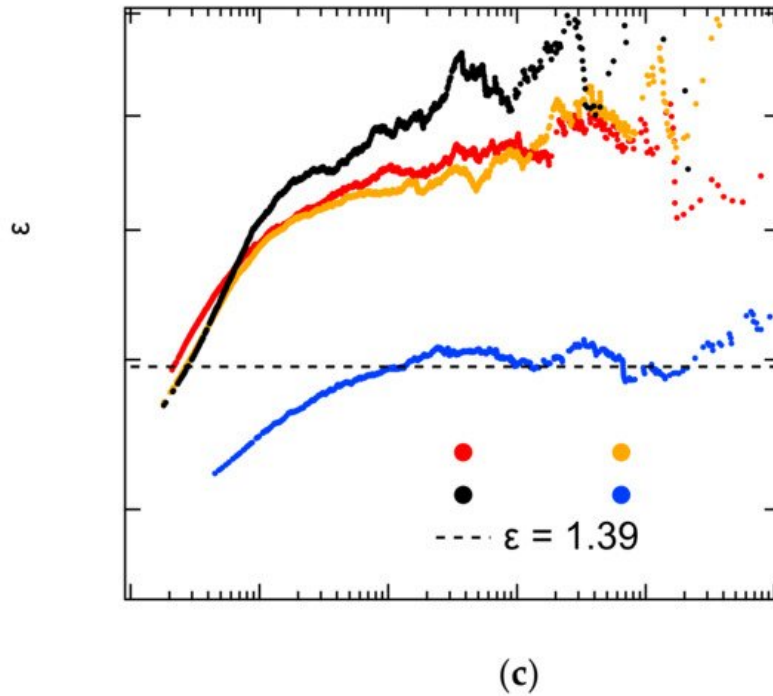

Figure 6. (**a**) AE energy spectra with a series of active periods, $n = 1, 2, 3$, and 4. The red continuous curve represents the energy average of 30 consecutive events. (**b**) Distribution of avalanche energies for $n = 1$ and $n = 4$ in creep experiments. (**c**) The ML-fitting exponent ε as function of the lower threshold E_{min} for $n = 1, 2, 3$, and 4. The horizontal dashed line ($\varepsilon = 1.39$) indicates the result from Vycor compression. Reproduced with permission from [54]. AIP Publishing, 2018.

Periodic changes of water levels in reservoirs causes wet cycle damage of reservoir rocks. The Three Gorges Reservoir was formed by the construction of China's Three Gorges Dam, the world's largest water conservancy project, which contains changes of water levels by nearly 30 m. Xie et al. used the typical sandstone in the Three Gorges Reservoir Area to measure acoustic emission and nuclear magnetic resonance images to study the dry–wet cycle damage [57]. The internal damage of sandstone caused by dry–wet cycles is best seen by nuclear magnetic imaging. The detailed relation between the AE energy distribution exponent and the number of wetting–drying cycles is shown in **Figure 7** , and the exponent values decreased in an exponential fashion towards the mean field value of 1.6.
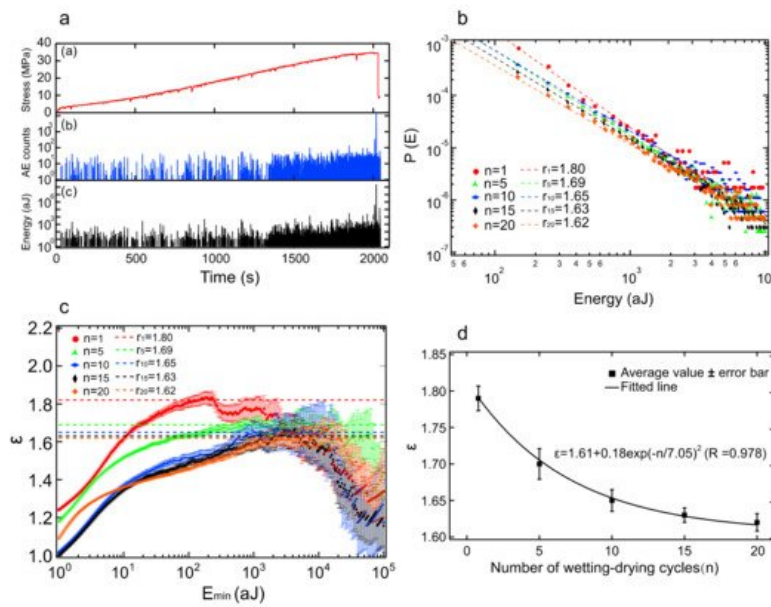
Figure 7. (**a**) AE spectra corresponding to stress curve in damaged sandstone. (**b**) The AE energies distribution of sandstone samples with different number of wetting–drying cycle in log–log scale. (**c**) the ML-fitting curves as a cutoff E_{min}, the plateau value is consistent with the slope in log–log scale. (**d**) the relationship between the energy exponent and the number of cyclic wetting events. Reproduced with permission from [57]. Springer Nature, 2018.

References

1. Ding, X.; Zhao, Z.; Lookman, T.; Saxena, A.; Salje, E.K.H. High junction and twin boundary densities in driven dynamical systems. Adv. Mater. 2012, 24, 5385–5389.

2. Chen, Y.; Ding, X.; Fang, D.; Sun, J.; Salje, E.K.H. Acoustic emission from porous collapse and moving dislocations in granular Mg-Ho alloys under compression and tension. Sci. Rep. 2019, 9, 1–12.

3. Salje, E.K.H.; Xue, D.; Ding, X.; Dahmen, K.A.; Scott, J.F. Ferroelectric switching and scale invariant avalanches in BaTiO3. Phys. Rev. Mater. 2019, 3, 014415.

4. Salje, E.K.H.; Li, S.; Stengel, M.; Gumbsch, P.; Ding, X. Flexoelectricity and the polarity of complex ferroelastic twin patterns. Phys. Rev. B 2016, 94, 024114.

5. Salje, E.K.; Soto-Parra, D.E.; Planes, A.; Vives, E.; Reinecker, M.; Schranz, W. Failure mechanism in porous materials under compression: Crackling noise in mesoporous SiO2. Philos. Mag. Lett. 2011, 91, 554–560.

6. Sethna, J.P.; Dahmen, K.A.; Myers, C.R. Crackling noise. Nature 2001, 410, 242.

7. Perković, O.; Dahmen, K.; Sethna, J.P. Avalanches, Barkhausen Noise, and Plain Old Criticality. Phys. Rev. Lett. 1995, 75, 4528–4531.

8. Dahmen, K.; Sethna, J.P. Hysteresis, avalanches, and disorder-induced critical scaling: A renormalization-group approach. Phys. Rev. B 1996, 53, 14872–14905.

9. Salje, E.; Dahmen, K.A. Crackling Noise in Disordered Materials. Annu. Rev. Condens. Matter Phys. 2014, 5, 233–254.

10. Salje, E.K.; Saxena, A.; Planes, A. Avalanches in Functional Materials and Geophysics; Springer: London, UK, 2017.

11. Bak, P.; Christensen, K.; Danon, L.; Scanlon, T. Unified Scaling Law for Earthquakes. Phys. Rev. Lett. 2002, 88, 178501.

12. Kawamura, H.; Hatano, T.; Kato, N.; Biswas, S.; Chakrabarti, B.K. Statistical physics of fracture, friction, and earthquakes. Rev. Mod. Phys. 2012, 84, 839–884.

13. Preziosi, D.; Lopez-Mir, L.; Li, X.; Cornelissen, T.; Lee, J.H.; Trier, F.; Bouzehouane, K.; Valencia, S.; Gloter, A.; Barthélémy, A.; et al. Direct mapping of phase separation across the metal–insulator transition of NdNiO3. Nano Lett. 2018, 18, 2226–2232.

14. Yu, S.; Wu, Y.; Jeyasingh, R.; Kuzum, D.; Wong, H.-S.P. An electronic synapse device based on metal oxide resistive switching memory for neuromorphic computation. IEEE Trans. Electron Devices 2011, 58, 2729–2737.

15. Zhu, L.Q.; Wan, C.J.; Guo, L.Q.; Shi, Y.; Wan, Q. Artificial synapse network on inorganic proton conductor for neuromorphic systems. Nat. Commun. 2014, 5, 1–7.

16. Cocchi, L.; Gollo, L.L.; Zalesky, A.; Breakspear, M. Criticality in the brain: A synthesis of neurobiology, models and cognition. Prog. Neurobiol. 2017, 158, 132–152.

17. Pajevic, S.; Plenz, D. Efficient Network Reconstruction from Dynamical Cascades Identifies Small-World Topology of Neuronal Avalanches. PLoS Comput. Biol. 2009, 5, e1000271.

18. Harrison, R.; Dunin-Borkowski, R.; Putnis, A. Direct imaging of nanoscale magnetic interactions in minerals. Proc. Natl. Acad. Sci. USA 2002, 99, 16556–16561.

19. Robinson, P.; Harrison, R.J.; McEnroe, S.A.; Hargraves, R.B. Lamellar magnetism in the haematite–ilmenite series as an explanation for strong remanent magnetization. Nature 2002, 418, 517–520.

20. Roberts, A.P.; Hu, P.; Harrison, R.J.; Heslop, D.; Muxworthy, A.R.; Oda, H.; Sato, T.; Tauxe, L.; Zhao, X. Domain State Diagnosis in Rock Magnetism: Evaluation of Potential Alternatives to the Day Diagram. J. Geophys. Res. Solid Earth 2019, 124, 5286–5314.

21. Durin, G.; Zapperi, S. The Barkhausen effect. Physics 2006, 13, 461.

22. Vives, E.; Ortin, J.; Manosa, L.; Rafols, I.; Perezmagrane, R.; Planes, A. Distributions of avalanches in martensitic transformations. Phys. Rev. Lett. 1994, 72, 1694.

23. Gallardo, M.C.; Manchado, J.; Romero, F.J.; del Cerro, J.; Salje, E.K.H.; Planes, A.; Vives, E.; Romero, R.; Stipcich, M. Avalanche criticality in the martensitic transition of Cu67.64Zn16.71Al15.65 shape-memory alloy: A calorimetric and acoustic emission study. Phys. Rev. B 2010, 81, 174102.

24. Weiss, J.; Richeton, T.; Louchet, F.; Chmelik, F.; Dobron, P.; Entemeyer, D.; Lebyodkin, M.; Lebedkina, T.; Fressengeas, C.; McDonald, R.J. Evidence for universal intermittent crystal plasticity from acoustic emission and high-resolution extensometry experiments. Phys. Rev. B 2007, 76, 224110.

25. Zapperi, S.; Vespignani, A.; Stanley, H.E. Plasticity and avalanche behaviour in microfracturing phenomena. Nature 1997, 388, 658–660.

26. Casals, B.; Nataf, G.F.; Pesquera, D.; Salje, E.K.H. Avalanches from charged domain wall motion in BaTiO3 during ferroelectric switching. APL Mater. 2020, 8, 5.

27. Casals, B.; van Dijken, S.; Herranz, G.; Salje, E.K.H. Electric-field-induced avalanches and glassiness of mobile ferroelastic twin domains in cryogenic SrTiO3. Phys. Rev. Res. 2019, 1, 032025.

28. Casals, B.; Nataf, G.; Salje, E. Avalanche criticality during ferroelectric/ferroelastic switching. Nat. Commun. 2021, 12, 1–7.

29. Salje, E.; Wruck, B. Specific-heat measurements and critical exponentsof the ferroelastic phase-transition in PB3(PO4)2 and PB3(P1-XASXO4)2. Phys. Rev. B 1983, 28, 6510.

30. Navas-Portella, V.; Corral, A.; Vives, E. Avalanches and force drops in displacement-driven compression of porous glasses. Phys. Rev. E 2016, 94, 033005.

31. Salje, E.K.H.; Dul'kin, E.; Roth, M. Acoustic emission during the ferroelectric transition Pm(3)over-barm to P4mm in BaTiO3 and the ferroelastic transition R(3)over-barm-C2/c in Pb3(PO4)2. Appl. Phys. Lett. 2015, 106, 152903.

32. Salje, E.K.H.; Lampronti, G.I.; Soto-Parra, D.E.; Baró, J.; Planes, A.; Vives, E. Noise of collapsing minerals: Predictability of the compressional failure in goethite mines. Am. Miner. 2013, 98, 609–615.

33. Salje, E.K.H.; Wang, X.; Ding, X.; Sun, J. Simulating acoustic emission: The noise of collapsing domains. Phys. Rev. B 2014, 90, 064103.

34. Zreihan, N.; Faran, E.; Vives, E.; Planes, A.; Shilo, D. Relations between stress drops and acoustic emission measured during mechanical loading. Phys. Rev. Mater. 2019, 3, 043603.

35. Casals, B.; Dahmen, K.A.; Gou, B.; Rooke, S.; Salje, E.K.H. The duration-energy-size enigma for acoustic emission. Sci. Rep. 2021, 11, 1–10.

36. Chi-Cong, V.; Weiss, J. Asymmetric damage avalanche shape in quasibrittle materials and subavalanche (aftershock) clusters. Phys. Rev. Lett. 2020, 125, 105502.

37. Vu, C.-C.; Plé, O.; Weiss, J.; Amitrano, D. Revisiting the concept of characteristic compressive strength of concrete. Constr. Build. Mater. 2020, 263, 120126.

38. Yang, Y.; Li, S.; Ding, X.; Sun, J.; Weiss, J.; Salje, E.K. Twisting of pre-twinned α-Fe nanowires: From mild to wild avalanche dynamics. Acta Mater. 2020, 195, 50–58.

39. Soto-Parra, D.E.; Zhang, X.; Cao, S.; Vives, E.; Salje, E.K.H.; Planes, A. Avalanches in compressed Ti-Ni shape-memory porous alloys: An acoustic emission study. Phys. Rev. E 2015, 91, 060401.

40. Salje, E.K.H.; Zhang, H.; Idrissi, H.; Schryvers, D.; Carpenter, M.A.; Moya, X.; Planes, A. Mechanical resonance of the austenite/martensite interface and the pinning of the martensitic microstructures by dislocations in Cu74.08Al23.13Be2.79. Phys. Rev. B 2009, 80, 134114.

41. Salje, E.K.H.; Jiang, X. Crackling noise and avalanches in minerals. Phys. Chem. Miner. 2021, 48, 1–15.

42. Salje, E.K.H.; Planes, A.; Vives, E. Analysis of crackling noise using the maximum-likelihood method: Power-law mixing and exponential damping. Phys. Rev. E 2017, 96, 042122.

43. Bauke, H. Parameter estimation for power-law distributions by maximum likelihood methods. Eur. Phys. J. B 2007, 58, 167–173.

44. Clauset, A.; Shalizi, C.R.; Newman, M.E.J. Power-Law Distributions in Empirical Data. SIAM Rev. 2009, 51, 661–703.

45. Alava, M.J.; Nukala, P.K.V.V.; Zapperi, S. Statistical models of fracture. Adv. Phys. 2006, 55, 349–476.

46. Salje, E.K.H.; Liu, H.; Xiao, Y.; Jin, L.; Planes, A.; Vives, E.; Xie, K.; Jiang, X. Avalanche mixing and the simultaneous collapse of two media under uniaxial stress. Phys. Rev. E 2019, 99, 023002.

47. Xie, K.N.; Jiang, X.; Jiang, D.; Xiao, Y.; Chen, S.; Dahmen, K.A.; Vives, E.; Planes, A.; Salje, E.K. Change of crackling noise in granite by thermal damage: Monitoring nuclear waste deposits. Am. Miner. 2019, 104, 1578–1584.

48. Zhao, Y.F.; Liu, H.; Xie, K.; Salje, E.K.; Jiang, X. Avalanches in compressed sandstone: Crackling noise under confinement. Crystals 2019, 9, 582.

49. Chen, Y.; Gou, B.; Fu, W.; Chen, C.; Ding, X.; Sun, J.; Salje, E.K.H. Fine structures of acoustic emission spectra: How to separate dislocation movements and entanglements in 316L stainless steel. Appl. Phys. Lett. 2020, 117, 262901.

50. Terzis, D.; Laloui, L. 3-D micro-architecture and mechanical response of soil cemented via microbial-induced calcite precipitation. Sci. Rep. 2018, 8, 1416.

51. De Jong, J.T.; Soga, K.; Kavazanjian, E.; Burns, S.; van Paassen, L.; Al Quabany, A.; Aydilek, A.; Bang, S.; Burbank, M.; Caslake, L.; et al. Biogeochemical processes and geotechnical applications: Progress, opportunities and challenges. Geotechnique 2013, 63, 287–301.

52. Wang, L.; Jiang, X.; He, X.; Chu, J.; Xiao, Y.; Liu, H.; Salje, E.K. Crackling noise and bio-cementation. Eng. Fract. Mech. 2021, 247, 107675.

53. Wang, L.; Cao, S.; Jiang, X.; Salje, E.K.H. Cracking of human teeth: An avalanche and acoustic emission study. J. Mech. Behav. Biomed. Mater. 2021, 122, 104666.

54. Salje, E.K.H.; Liu, H.; Jin, L.; Jiang, D.; Xiao, Y.; Jiang, X. Intermittent flow under constant forcing: Acoustic emission from creep avalanches. Appl. Phys. Lett. 2018, 112, 054101.

55. Kun, F.; Halasz, Z.; Andrade, J.S., Jr.; Herrmann, H.J. Crackling noise in sub-critical fracture of heterogeneous materials. J. Stat. Mech. Theory Exp. 2009, 2009, P01021.

56. Halász, Z.; Danku, Z.; Kun, F. Competition of strength and stress disorder in creep rupture. Phys. Rev. E 2012, 85, 016116.

57. Xie, K.; Jiang, D.; Sun, Z.; Chen, J.; Zhang, W.; Jiang, X. NMR, MRI and AE Statistical Study of Damage due to a Low Number of Wetting–Drying Cycles in Sandstone from the Three Gorges Reservoir Area. Rock Mech. Rock Eng. 2018, 51, 3625–3634.